

Cite this: *Photochem. Photobiol. Sci.*, 2019, **18**, 1512

A dual-mode highly selective and sensitive Schiff base chemosensor for fluorescent colorimetric detection of Ni²⁺ and colorimetric detection of Cu²⁺†

Amit Kumar Manna,^a Kalyani Rout,^a Shubhamoy Chowdhury^b and Goutam K. Patra *^a

In this paper, a novel flexible Schiff base chemosensor *N'*-(2-hydroxy-3-methoxybenzylidene)-2-(benz-amido)benzohydrazide (**L**) has been designed, synthesised and characterised by ¹H-NMR, IR spectroscopy, ESI-MS spectrometry and single crystal XRD analysis. A significant fluorescence enhancement of **L** was observed only in the presence of Ni²⁺ ions with a detection limit of 3.64 μM whereas Cu²⁺ induced fluorescence quenching, although both the metals showed colorimetric responses in methanol–Tris–HCl buffer (10 mM, pH 7.2) solution (1 : 1, v/v). The single crystal structure of **L**–Cu²⁺ has also been determined. No major interference by the other effective background cations (Fe³⁺, Fe²⁺, Co²⁺, Zn²⁺, Cd²⁺, Hg²⁺, Pb²⁺, Cr³⁺, Ag⁺, Al³⁺ and Mn²⁺) was observed even at a higher concentration of analytes. The experimental results were further supported by DFT studies. The chemosensor **L** can be applied to the formation of binary logical devices, recovery of contaminated water samples and living intracellular media.

Received 10th March 2019,
Accepted 1st April 2019

DOI: 10.1039/c9pp00114j

rsc.li/pps

Introduction

The ion detection properties of an effective chemosensor mainly depend on host–guest binding affinities promoted by non-covalent interactions like metal–ligand complexation, hydrogen bonding interaction, van der Waals interactions and change in the optical or electrochemical properties of the system.^{1,2} Several standard methods such as potentiometry,³ chromatography,⁴ atomic absorption spectroscopy (AAS),⁵ inductively coupled plasma emission spectroscopy (ICP-ES),⁶ inductively coupled plasma mass spectroscopy (ICPMS),⁷ and flow injection amperometry⁸ are also available but these techniques include serious drawbacks like troublesome sample preparation, necessity of trained personnel, expensive and sophisticated instruments, and careful operation and time consumption.⁹ In recent years, an optical chemosensor has been extensively used as an alternative approach to detect and

quantify these analytes due to its operational simplicity, high sensitivity, better selectivity, reproducibility, less sample and time consumption and a real time process.^{10–12}

After Fe and Zn, Cu is the 3rd most important essential trace element in biological systems. It acts as an essential constituent of several proteins and enzymes *e.g.* super oxide dismutase, cytochrome *c*-oxidase, ceruloplasmin, tyrosinase and nuclease.^{13,14} It also plays a significant role in several fundamental physiological processes like iron utilisation and haemoglobin formation.^{15,16} Despite its vital roles, an excess intake of Cu²⁺ can cause toxic effects due to the formation of harmful reactive oxygen species (ROS) which results in liver or kidney damage and neuro-degenerative disorder like Wilson's disease, Parkinson's disease, Alzheimer's disease and Mcknes syndrome.^{17–22} Like Cu²⁺ ions, Ni²⁺ also plays an essential role in several biological processes such as respiration, metabolism and biosynthesis. It is also present in the active sites of several metallo-enzymes, for example hydrogenases, carbon monoxide dehydrogenases and acireductone deoxygenases.^{23–25} Due to its widespread metallurgical application in industrial processes such as Ni–Cd batteries, electroplating, electroforming, and alloy production,^{26,27} Ni²⁺ can easily enter into the aquatic ecosystem and cause negative impacts to the environment. Overloading of Ni²⁺ in the human body results in numerous adverse effects, including allergy, respiratory problems, pneumonitis, lung cancer, central nervous system disorders *etc.*^{28,29}

^aDepartment of Chemistry, Guru Ghasidas Vishwavidyalaya, Bilaspur, C.G, India.
E-mail: patra29in@yahoo.co.in; Tel: +91 7587312992

^bDepartment of Chemistry, GourBanga University, Malda, West Bengal 732 103, India

†Electronic supplementary information (ESI) available: Tables S1–S6 and Fig. S1–S14. CCDC 1864565 and 1864566 for probe **L** and complex **1**. For ESI and crystallographic data in CIF or other electronic format see DOI: 10.1039/c9pp00114j

So there is an urgent need to maintain the balance of these toxic metal ions in biological and environmental systems.

Generally, Schiff bases provide suitable geometrical and electronic environment towards some selected metal ions providing stable host-guest interaction. As the specific ion selectivity is dependent on the relative stability of host-guest adduct formation and controlled by the structural features of the receptor and the optical signal is due to influence of guest on the electronic environment of host,³⁰ numerous chemoreceptor has been developed using multi-dentate Schiff base scaffolds. Although several reports are available based on a Schiff base chemosensor citing Ni²⁺ and Cu²⁺ ions separately,^{31,32} the dual sensing mode is still limited. However, multiple analyte detection by a single molecular probe is cost effective and a less time consuming process, and thus has been highly desirable in recent times. Optical methods based on colorimetric receptors are especially attractive due to real time analysis, simplicity and low capital cost as compared to fluorescence where UV radiation and more sophisticated instruments are required,³³ although the latter has more sensitivity than the former.³⁴ Furthermore, quenching of the emission intensity occurs by the paramagnetic Ni²⁺ and Cu²⁺ ions through the excited state electron/energy transfer process but such a mechanism is less prominent in optical measurement due to its false pulse. Thus development of a *turn on* chromogenic Schiff base probe is more essential for rapid detection of Ni²⁺ and Cu²⁺ ions at trace levels.

Based on the above facts and in continuation of our current research interest,³⁵ we have developed the novel Schiff base receptor **L**, by condensation of *o*-vanillin with one synthesised amine, 3-amino-2-phenyl-4(3*H*)-quinazolinone, for the selective detection of Ni²⁺ and Cu²⁺ ions in aqueous medium. Here, considering the requirement of the flexible coordination sites, we have modified the heterocyclic quinazolinone ring structure through the introduction of multiple C=O and -OH donor centres along with an electron rich C=N moiety in the skeleton of the chemosensor **L** for appropriate complexation. The probe **L** shows apparent colour and absorption changes in the presence of both Ni²⁺ and Cu²⁺ ions, whereas it shows fluorogenic response only towards Ni²⁺ ions. Schiff bases originating from *o*-hydroxy substituted aldehydes induce large Stokes shifts through a six-membered stable excited state intramolecular proton transfer (ESIPT) process. The proposed sensing mechanism has further been confirmed by FTIR, ¹H-NMR, ESI-MS spectroscopy and DFT studies. The structures of the chromophore **L** and its Cu(II) complex (**1**) have been confirmed by X-ray single crystal analysis. The structure of the Ni(II) complex (**2**) has been derived from DFT studies. The proposed chemosensor **L** is applicable in real sample analysis, living cell imaging and building of molecular logic gates.

Experimental

Materials and general information

All the required materials used for synthesis were obtained from Sigma-Aldrich and used as received. Analytical grade sol-

vents were used for the overall experiments and freshly prepared double deionized water was used for the dilution purpose and preparing methanol-Tris-HCl buffer (10 mM, pH 7.2) solution (1 : 1, v/v). The metal ion solutions were prepared from their nitrate salts and the solutions of anions were prepared from their sodium salts. ¹H NMR and ¹³C NMR spectra were recorded on a Bruker DRX spectrometer operating at 400 MHz in CDCl₃ and chemical shifts were recorded in ppm relative to TMS. Absorption spectra were recorded on a Shimadzu UV 1800 spectrophotometer using 10 mm path length quartz cuvettes with the wavelength in the range of 200–800 nm. High resolution mass spectra (HRMS) were recorded on a Waters mass spectrometer using a mixed solvent of HPLC methanol and triple distilled water. The pH measurements were done using a digital pH meter (Merck) by adjusting dilute hydrochloric acid and sodium hydroxide in buffer solution. The solutions of the receptor **L** (1 × 10⁻⁵ M) and metal salts (1 × 10⁻⁴ M) were prepared in CH₃OH and H₂O respectively.

X-ray data collection and structural determination

X-ray single crystal data were collected using MoK α (λ = 0.7107 Å) radiation on a BRUKER APEX II diffractometer equipped with a CCD area detector. Data collection, data reduction, and structure solution/refinement were carried out using the software package of SMART APEX.³⁶ The structures were solved by direct methods (SHELXS-97) and standard Fourier techniques, and refined on *F*² using full matrix least squares procedures (SHELXL-97) using the SHELX-97 package³⁷ incorporated in WinGX.³⁸ In most of the cases, non-hydrogen atoms were treated anisotropically. Hydrogen atoms were fixed geometrically at their calculated positions following a riding atom model. The crystallographic data of **L** and its copper complex (**1**) are listed in Table 1. Structural information of **L** and **1** has been deposited at the Cambridge Crystallographic Data Center (CCDC 1831118 and 1843677 respectively).

Synthesis of *N*-(2-hydroxybenzylidene)-2-(benzamido) benzohydrazide (**L**)

3-Amino-2-phenyl-4(3*H*)-quinazolinone (**3**) was prepared by a reported procedure.^{35a} 0.237 g (1 mmol) of this synthesized amine “**3**” was dissolved in 10 mL of dehydrated methanol, and a catalytic amount of glacial acetic acid was added to this solution. Next, 5 mL methanolic solution of 0.152 g (1 mmol) *o*-vanillin was added dropwise and the reaction mixture was refluxed for 2 h under dry conditions. The resulting mixture was kept in air for 24 h. The crystalline solid separated out was filtered, washed with methanol and dried in air. Yield, 0.323 g, 83%; mp. >200 °C. Single crystals suitable for X-ray analysis were obtained from the slow evaporation of the methanol solution of **L**. Anal. Calc. for C₂₂H₁₉N₃O₄: C, 67.86; H, 4.92; N, 10.79. Found C, 67.71; H, 4.87; N, 10.68%. EI-MS: *m/z* 412.12 (M + Na⁺, 100%) (Fig. S1†). FTIR/cm⁻¹ (KBr): 3475 (wb), 3210 (b, -NH), 3066 (m, aromatic CH- str), 1664 (vs, C=O), 1612 (vs, C=N), 1515 (s), 1450 (s), 1312 (m), 1298 (s), 1083 (s), 709

Table 1 Crystallographic data and refinement parameters of the probe **L** and complex **1**

Compound	L	1
Formula	C ₂₂ H ₁₉ N ₃ O ₄	C ₂₃ H ₂₁ N ₃ O ₅ Cu
Formula weight	389.40	482.08
Crystal system	Orthorhombic	Monoclinic
Space group	<i>Pn</i> (7)	<i>C</i> 12/ <i>c</i> 1 (15)
<i>a</i> (Å)	8.559(4)	26.093(12)
<i>b</i> (Å)	24.701(9)	11.611(5)
<i>c</i> (Å)	17.801(8)	14.522(5)
α [°]	90	90
β [°]	90	106.229(14)
γ [°]	90	90
<i>V</i> [Å ³]	3763.3(16)	4224.1(15)
<i>Z</i>	2	8
<i>D</i> (calc.) [g cm ⁻³]	1.369	1.579
μ (MoK α) [mm ⁻¹]	0.096	1.082
<i>F</i> (000)	1620	2080
Temperature (K)	293(2)	293(2)
Radiation [Å] (MoK α)	0.71073	0.71073
Theta min-max [°]	2.166, 26.605	1.708, 23.790
<i>N</i> _{ref}	7842	3151
<i>N</i> _{par}	1064	313
<i>R</i>	0.0788	0.0773
<i>wR</i> ₂	0.2611	0.2360
<i>S</i>	0.940	0.843
CCDC	1864565	1864566

(s) (Fig. S2†). ¹H NMR (400 MHz, DMSO, TMS): δ 12.29 (s, OH), 11.91 (s, 1H, NH), 10.74 (s, 1H, NH), 8.70 (s, 1 H, azomethine), 8.5–6.83 (m, 12H, aromatic), 3.82 (s, 3H, OMe) (Fig. S3†).

Synthesis of [CuL(OCH₃)] (**1**)

A methanolic solution (10 mL) of Cu(NO₃)₂·3H₂O (0.120 g, 0.5 mmol) was added dropwise with stirring to a solution of **L** (0.195 g, 0.5 mmol) in methanol (20 mL). The mixture was stirred for an additional 3 h and then the bluish-green precipitate was collected by filtration, washed with methanol and hexane. Slow evaporation of the methanol solution of this bluish green solid yielded a crystalline solid (suitable for X-ray analysis). Yield, 72%. Anal. Calc. for C₂₃H₂₁CuN₃O₅: C, 57.20; H, 4.38; N, 8.70%. Found C, 57.15; H, 4.30; N, 8.77%. EI-MS: *m/z* 482.11 (M + Cu²⁺ + OCH₃). FTIR/cm⁻¹ (KBr): 3440 (–NH), 3024 (m, aromatic CH– str), 1660 (vs, C=O), 1606 (vs, C=N), 1504 (s), 1443 (m), 1385 (s), 1313 (s), 1216 (s), 1167 (s), 1037 (m), 708 (s).

Synthesis of [NiL(OH₂)]NO₃ (**2**)

A similar method to the synthetic procedure of **1** was adopted for the synthesis of **2**. Ni(NO₃)₂·6H₂O was used in place of Cu(NO₃)₂·3H₂O. Yield, 78%. Anal. Calc. for C₂₂H₂₀NiN₄O₈: C, 50.13; H, 3.82; N, 10.62. Found C, 50.22; H, 3.75; N, 10.70%. EI-MS: *m/z* = 465.14 (L + Ni²⁺ + H₂O). FTIR/cm⁻¹ (KBr): 3445 (–NH), 3300 (–OH), 1645 (vs, C=O), 1602 (vs, C=N), 1525 (s), 1507 (m), 1440 (m), 1345 (s, NO₃⁻ stretching), 1252 (s), 706 (s).

Photophysical measurement

Chemosensor **L** (3.89 mg) was dissolved in 10 mL of CH₃OH to make a solution of 1 × 10⁻³ M and 30 μ L of this solution were

diluted with 2.97 mL of the CH₃OH–Tris–HCl buffer (1 : 1 v/v) mixture to make a final concentration of 10 μ M. The stock solutions of various metal ions were prepared separately from their nitrate salts (except sulphate salts of Mn²⁺ and Fe²⁺) at a concentration of 1 × 10⁻³ M in 10 mL double-deionised water and further diluted to their desired concentrations. After mixing **L** with each of the metal ions for a few seconds, absorption and fluorescence spectra were obtained at room temperature.

Job's plot measurements

A methanol–Tris–HCl buffer (10 mM, pH 7.2) solution (1 : 1, v/v) containing **L** (10 μ M) and an aqueous solution of Cu(NO₃)₂ and Ni(NO₃)₂ (10 μ M each) were prepared separately. Then the mole ratio of **L** was changed from 0.1 to 0.9 in such a manner that the sum of the total metal ion and **L** volume remained constant (2 mL). All the solutions were diluted to 3 mL. After shaking them for a minute, UV-vis spectra were obtained at room temperature.

Computational details

The GAUSSIAN-09 Revision C.01 program package was used for all calculations.³⁹ The gas phase geometries of molecules **L**, **1** and **2** were optimized fully by unrestricting of symmetry in singlet, doublet and singlet ground states respectively with the B3LYP functional.⁴⁰ The basis set LANL2DZ with an effective core potential (ECP) was used for copper and nickel following the associated valence double ζ basis set of Hay and Wadt.⁴¹ This is in combination with the 6-31++G** basis set selected for hydrogen, carbon, nitrogen and oxygen atoms.⁴² The same basis sets and functional were used for the calculation of vibrational frequencies. The HOMOs and LUMOs of molecules **L**, **1** and **2** were calculated with the TD-DFT method, and the solvent effect (in methanol for **L** and **1** and the aqueous solution for **2**) was simulated using the polarizing continuum model with the integral equation formalism (C-PCM).^{43,44}

Cell imaging study

Human cervical cancer cells, HeLa, were selected for the study. They were grown in Dulbecco's modified Eagle's medium (DMEM) and supplemented with 10% Fetal Bovine Serum (FBS), and a 1% antibiotic mixture containing PSN (Gibco BRL) at 37 °C in a humidified incubator with 5% CO₂. For the cell imaging study the cells were seeded in a 35 mm culture dish with a seeding density of 3 × 10⁵ cells per dish. Cells were grown to 80–90% confluence, harvested with 0.025% trypsin (Gibco BRL) and 0.52 mM EDTA (Gibco BRL) in phosphate buffered saline (PBS) and allowed to re-equilibrate for 24 h before any treatment. All experiments were conducted in DMEM containing 10% FBS and 1% PSN antibiotic. Cells were washed with PBS and then incubated with DMEM-containing 20 μ M chemosensor **L** [20 μ M in DMEM, DMSO : water = 1 : 9 (v/v), pH 7.2 in PBS buffer] for 1 h at 37 °C. It was left for another incubation by adding 40 μ M of nickel nitrate and then fluorescence images were taken by using a fluorescence microscope (Model: LEICA DMLS) with an objective lens of 20× mag-

nification with an excitation of 350–360 nm and an emission of 470 nm.

Results and discussion

Synthesis and structure of L

The Schiff base chemosensor **L** was successfully synthesized by the condensation reaction of amine '3' with *o*-vanillin with a high yield (over 80%) (Scheme 1). It was characterised by standard solution based analytical techniques like ESI-mass and ^1H NMR and solid studies like elemental analysis, IR spectroscopy and single crystal XRD analysis.

The single crystals of the probe *N*-(2-hydroxybenzylidene)-2-(benzamido)benzohydrazide (**L**) were grown by slow evaporation of the methanol solution at room temperature. **L** was crystallized as the orthorhombic $Pn(7)$ space group. There are four independent molecules present in the asymmetric unit of **L**. The ORTEP diagram of **L** has been shown in Fig. 1. In **L**, the bond lengths and angles are in the expected ranges. Intermolecular N–H...N and C–H...O hydrogen bonding interactions are present in the crystal structure.

Spectroscopic studies of L towards different metal ions

The metal ion chelating ability of receptor **L** was initially investigated visually and by UV-Vis spectral studies in methanol–Tris-HCl buffer (10 mM, pH 7.2) solution (1 : 1, v/v) at room temperature. The free receptor **L** displays the main absorption peak around 295 nm which may be due to a S_0 – S_1 transition. With the addition of 2 equiv. of different metal ions (Fe^{3+} , Cu^{2+} , Co^{2+} , Ni^{2+} , Zn^{2+} , Cd^{2+} , Hg^{2+} , Pb^{2+} , Cr^{3+} , Ag^+ , Al^{3+} , Mn^{2+} and Fe^{2+}) individually, new absorption bands emerged at 402 and 420 nm, respectively, only in the case of the addition Cu^{2+} and Ni^{2+} ions, whereas no other metal ions showed any significant change in absorption under these conditions (Fig. 2a). As a consequence, the pale yellow colour of the **L** solution changes into intense yellow in the presence of both the metal ions (Cu^{2+} and Ni^{2+}). Then, the specific Cu^{2+} and Ni^{2+} ion selective responses of the chemosensor **L** were investigated by absorption spectral studies under the same experimental conditions. The co-existence of similar concentrations of other major competing cations with Cu^{2+} and Ni^{2+} ions, individually, cannot disturb the absorbance band of the guest bound recep-

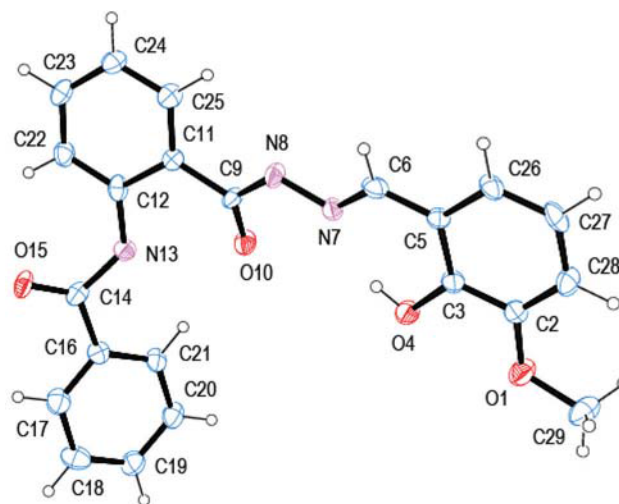
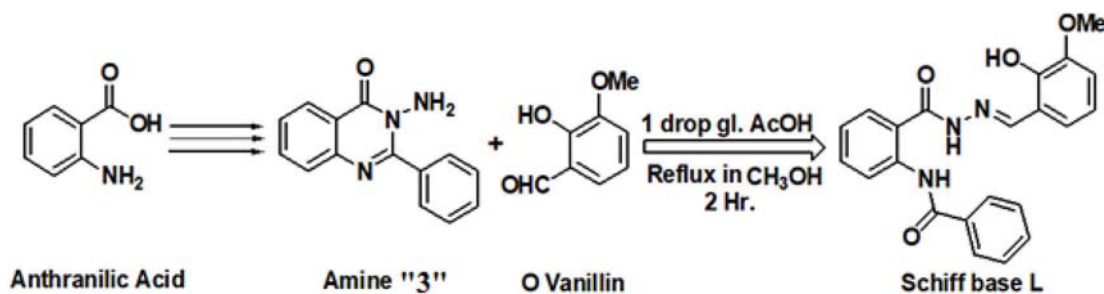


Fig. 1 ORTEP diagram of the receptor **L** with 40% ellipsoid.

tor above 400 nm. This anti-interference behaviour was also consistent even up to 5-fold higher concentrations of background cations with respect to each analyte concentration, confirmed by neither the generation of an extra peak nor the disappearance of the original peak of the host–guest complex (Fig. 2b). Moreover, an equivalent concentration of Cu^{2+} ions can replace Ni^{2+} from the **L**– Ni^{2+} complex solution, and thus the absorbance band analogous to the **L**– Cu^{2+} complex was observed.

In order to investigate the detailed aspect of the insight mechanism, absorption titration experiments were conducted independently in methanol–tris-HCl buffer (10 mM, pH 7.2) solution (1 : 1, v/v). In the metal free state, the receptor displayed the main absorption band around 295 nm which may be attributed to the π – π^* transition along with a broad shoulder peak at 320 nm assigned for the internal charge transfer (ICT) process throughout the molecule which gives a pale yellow solution. Upon stepwise increasing of analyte concentration, two intense absorption bands appeared at 250 and 402 nm for Cu^{2+} (Fig. 3a) and a new absorption band appeared at 420 nm for Ni^{2+} (Fig. 3b). Except in the first step of addition, the absorption band at 295 nm goes on decreasing consistently and reaches the saturation point with 1 equiv. of Cu^{2+} and 1.5 equiv. of Ni^{2+} ions. Also isosbestic points were



Scheme 1 Synthetic procedure of the probe **L**.

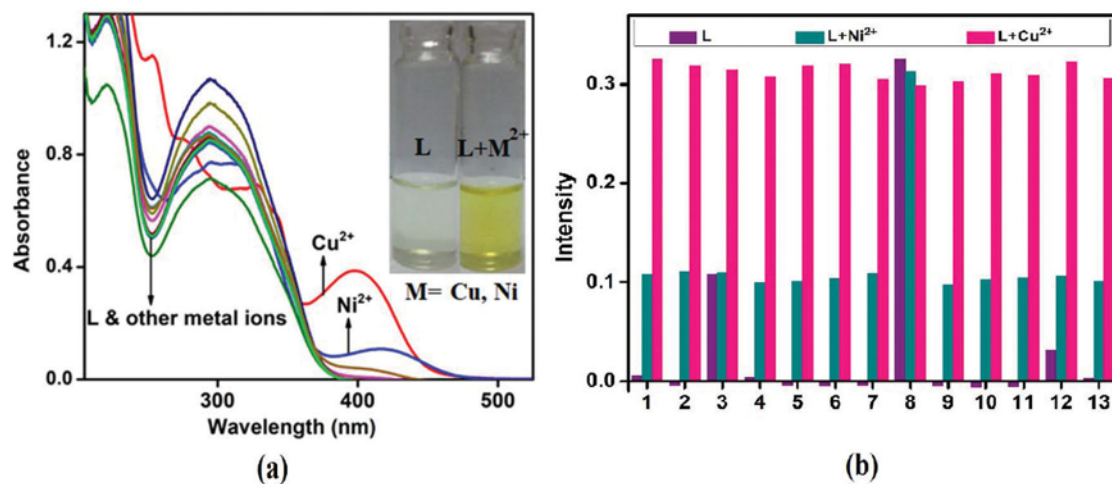


Fig. 2 (a) Absorption spectra of L (10 μM) change in the presence of 2 equiv. of different metal ions. Inset: Colour change of L on addition of 2 equiv. of M^{2+} ($\text{M} = \text{Ni}$ and Cu). (b) Competitive experiment in the presence of L and other metal ions (where 1 = L, 2 = Fe^{3+} , 3 = Ni^{2+} , 4 = Co^{2+} , 5 = Cd^{2+} , 6 = Hg^{2+} , 7 = Pb^{2+} , 8 = Cu^{2+} , 9 = Ag^+ , 10 = Al^{3+} , 11 = Mn^{2+} , 12 = Cr^{3+} and 13 = Zn^{2+}).

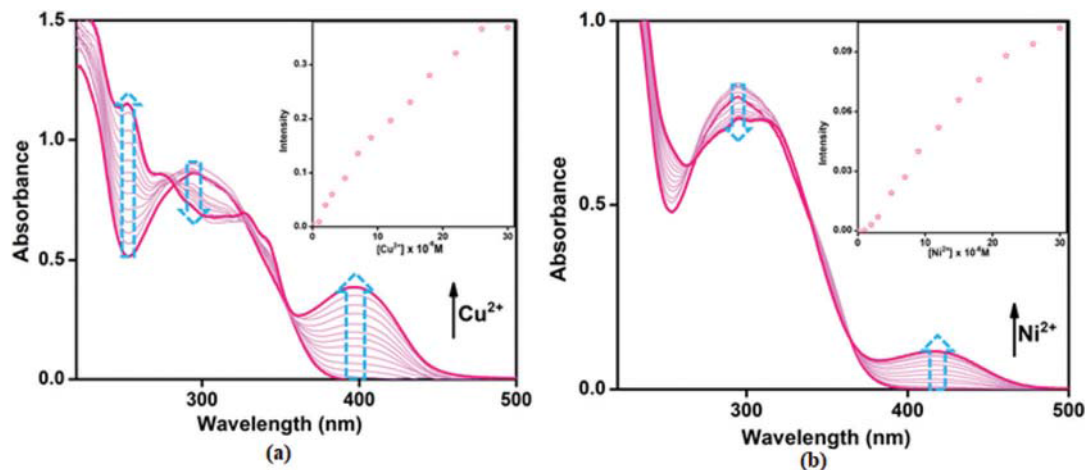


Fig. 3 UV-vis titration of L with (a) Ni^{2+} and (b) Cu^{2+} in methanol-Tris-HCl buffer (10 mM, pH 7.2) solution (1 : 1, v/v). Inset: Plot of intensity vs. concentration of the analytes.

observed at 353 and 364 nm for Cu^{2+} and Ni^{2+} ions respectively (Fig. 3), which confirmed that both L and $\text{L} + \text{M}^{2+}$ ($\text{M} = \text{Cu}$ and Ni) are in dynamic equilibrium.

The sensitivity curves for Cu^{2+} and Ni^{2+} were obtained from the titration profiles by varying the absorbance intensity with analyte amounts. To avoid several environmental interfering effects like photobleaching, pH, temperature, receptor concentration and to increase the dynamic range of the chemosensor, ratiometric measurement of the receptor L was also conducted by correlating the intensity ratio at two different wavelength regions ($I_{402/295}$ and $I_{420/295}$ for Cu^{2+} and Ni^{2+} respectively) with the incremental analyte concentration. These plots are almost sigmoidal and linear up to 26 μM for Cu^{2+} and 22 μM for Ni^{2+} (Fig. 4). The detection limits are calculated to be 1.89 μM for Cu^{2+} and 1.71 μM for Ni^{2+} ions, from the linear fitting of the ratiometric calibration curves using the formula, $\text{DL} = 3 \text{ SD } m^{-1}$,

where SD is the standard deviation of the blank measurements and m is the slope of the calibration curves, which are far below the guideline provided by the WHO in drinking water and several reported Cu^{2+} and Ni^{2+} sensors.

The host-guest binding stoichiometries can be determined from Job's plot analysis, which revealed that bindings for both the metal complexes occur in a 1 : 1 fashion (Fig. S4[†]). This observation is also in agreement with the results obtained from the ESI-MS spectral analysis of each $\text{L} + \text{M}^{2+}$ complex. In the positive ion mass spectrum, the peak at $m/z = 482.10$ was assignable to $\text{L} + \text{Cu}^{2+} + \text{OME}$ (Fig. S5[†]) and the peak at $m/z = 465.14$ was assignable to $\text{L} + \text{Ni}^{2+} + \text{H}_2\text{O}$ (Fig. S6[†]). Assuming a 1 : 1 binding ratio, the association constants towards the respective analytes were also calculated from the linear fitting of the Benesi-Hildebrand (B-H) graph and the values are $1.39 \times 10^4 \text{ M}^{-1}$ for $\text{L} + \text{Cu}^{2+}$ and $1.10 \times 10^4 \text{ M}^{-1}$ for $\text{L} + \text{Ni}^{2+}$

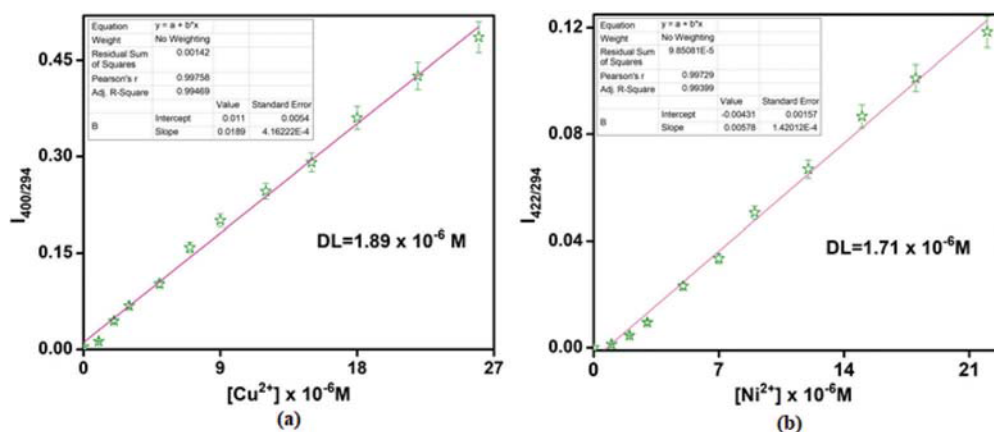


Fig. 4 Detection limits of L for (a) Cu^{2+} and (b) Ni^{2+} by ratiometric measurements.

(Fig. S7[†]), which are highly in agreement with the $\text{L} + \text{M}^{2+}$ complexes.

pH effect

The spectroscopic properties of chemosensor **L** can be influenced by the pH of the working media, as they contain several acid–base sensitive groups ($>\text{C}=\text{O}$, $>\text{C}=\text{N}$, $-\text{NH}$ and $-\text{OH}$). Thus to estimate the role of pH on complexation, different sets of pH solutions ranging from 3 to 13 have been prepared in separate vials by adjusting HCl and NaOH in the presence of a buffer solution so that each aliquot contains equal concentrations of $\text{L}-\text{M}^{2+}$ complexes (where $\text{M} = \text{Cu}$ and Ni). The absorption spectra of different pH solutions were recorded at room temperature (Fig. 5). The absorbance intensity of each of the receptors as well as their metal complexes decrease at lower pH values in contrast to the higher pH values indicating that the protonated form of coordination sites binds less effectively with the Cu^{2+} and Ni^{2+} ions in the acidic medium.

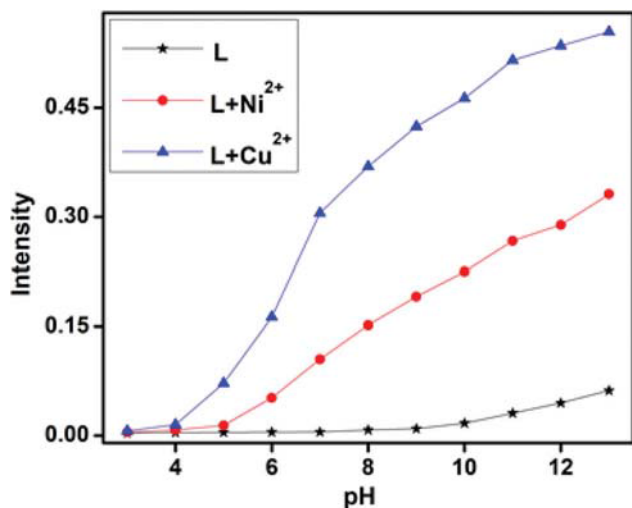


Fig. 5 pH effect of L, $\text{L}-\text{Cu}^{2+}$ (1) and $\text{L}-\text{Ni}^{2+}$ (2) at 405 nm.

Reversibility test

The reversible nature of the chemosensor **L** has been investigated by using a common metal chelator disodium ethylene diamine tetra acetic acid (Na_2EDTA). The absorption bands around 402 nm ($\text{L}-\text{Cu}^{2+}$) and 420 nm ($\text{L}-\text{Ni}^{2+}$) immediately vanished with the appearance of the original absorption band of **L**, when each $\text{L} + \text{M}^{2+}$ ($\text{M} = \text{Cu}$ and Ni) ensemble was treated with Na_2EDTA (Fig. 6). Consistent with the absorption band shift, the colour of the solution also changes from deep yellow to pale yellow in both the cases giving an indication of Cu^{2+} -EDTA and Ni^{2+} -EDTA complex formation leaving the sensor **L** free. Upon excessive addition of respective metal ions, the colour and spectral change almost recovered. The switching behaviour between **L** and $\text{L} + \text{M}^{2+}$ complexes ($\text{M} = \text{Cu}$ and Ni) was systematic even after several cycles with the alternative addition of the chelator and analytes. Cysteine participates frequently by binding with only the Cu^{2+} ion, thus it can be used in the sensing of Ni^{2+} ions in the presence of Cu^{2+} , and excessive addition of cysteine has no effect on Ni^{2+} ion detection (Fig. S8[†]). Thus the chemosensor **L** is reversible and the sensing process is recyclable.

Fluorescence experiment

The selective fluorometric behaviour of the receptor **L** towards metal ions was also investigated in methanol–Tris–HCl buffer (10 mM, pH 7.2) solution (1 : 1, v/v). For this purpose separate aliquots were prepared, containing a mixture of a constant amount of **L** and 2 equivalents of different metal ions like Fe^{3+} , Cu^{2+} , Co^{2+} , Ni^{2+} , Zn^{2+} , Cd^{2+} , Hg^{2+} , Pb^{2+} , Cr^{3+} , Ag^+ , Al^{3+} , Mn^{2+} and Fe^{2+} and the fluorescence spectra were recorded (Fig. 7). The free receptor **L** showed weak emission at 450 nm on excitation at 350 nm. Only Ni^{2+} ions induced a remarkable enhancement in the intensity as well as the position of the emission band, and the Cu^{2+} ions displayed quenching of fluorescence, whereas other selected metal ions can cause negligible fluorescence change even up to a 3-fold higher concentration than Ni^{2+} . The weak emission of the free receptor can be ascribed to the combinational effect of the photoinduced

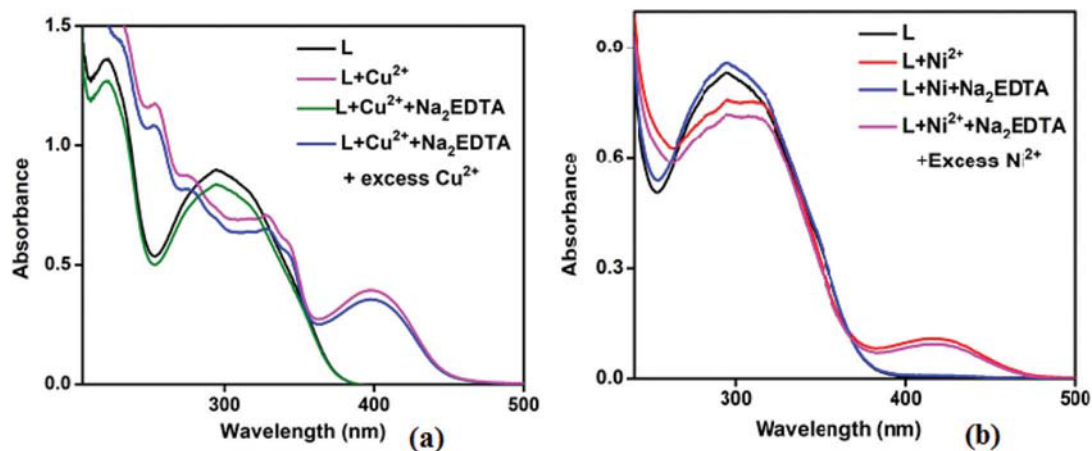


Fig. 6 Reversibility study of (a) L-Cu²⁺ and (b) L-Ni²⁺ complexes with Na₂EDTA.

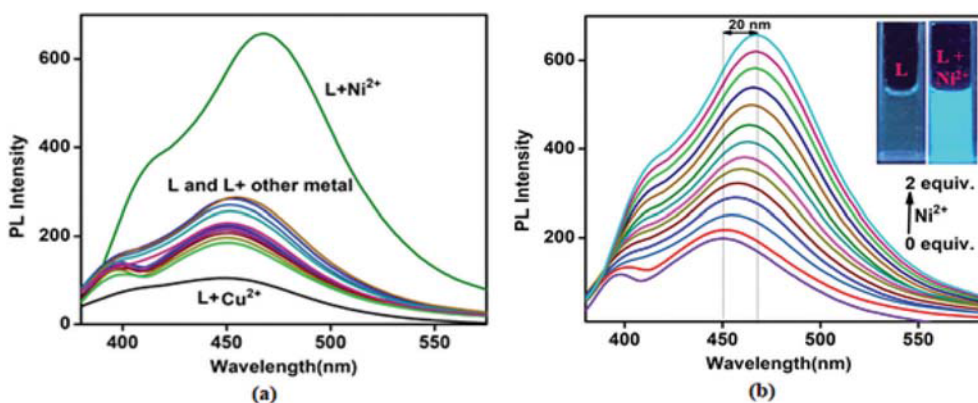


Fig. 7 (a) Fluorescence spectra of L in the presence of 2 equiv. of different metal ions and (b) fluorescence titration of L with Ni²⁺ in methanol-Tris-HCl buffer (10 mM, pH 7.2) solution (1 : 1, v/v).

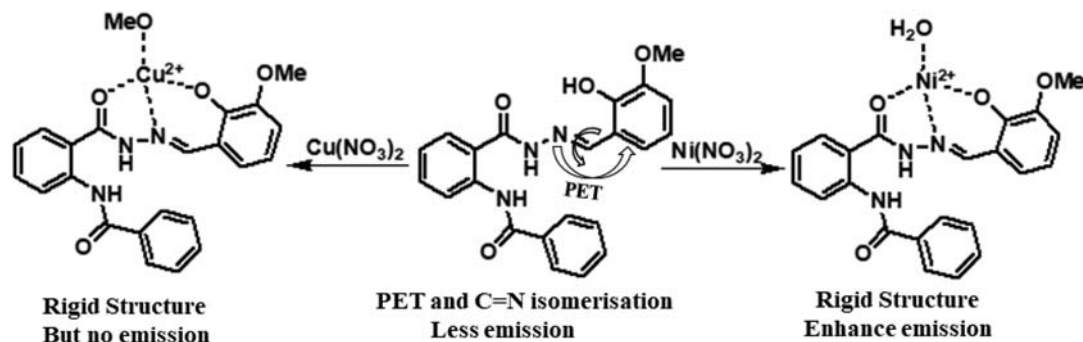
electron transfer (PET) and the excited state intramolecular proton transfer (ESIPT) mechanism. The free imine (>C=N) group participates in the PET process and the presence of a free -OH moiety at a suitable position causes a six-membered stable intramolecular proton transfer in the excited state which showed two emission bands at 395 (a small hump) and 450 nm. Initially the receptor L is quite flexible and undergoes *cis-trans* >C=N isomerisation. As soon as the Ni²⁺ ion co-ordinates through the imine and -OH donor sites, both PET and ESIPT processes diminish and strong chelation enhancement fluorescence occurs due to the blocking of the >C=N isomerisation process (Scheme 2). In the presence of Cu²⁺ ions, L showed the quenching mechanism due to its strong paramagnetic nature.

In order to obtain the quantitative sensitive response, fluorescence titration experiments were conducted under the same working conditions (Fig. 7b). Upon gradual addition of Ni²⁺ ions to the receptor solution, the intensity of the emission band at 450 nm increased with a red shift of about 20 nm, and 2 equiv. of Ni²⁺ ions were sufficient to saturate the enhanced emission band. The fluorometric detection limit was calcu-

lated to be 3.64×10^{-6} M from the linear fitting between the maximum PL intensity at 470 nm and the Ni²⁺ concentration using the same equation $DL = 3 SD m^{-1}$ (Fig. S9†). In the competitive experiments, the same concentration of the Cu²⁺ ion can cause quenching of the L-Ni²⁺ complex whereas other interfering metal ions show a negligible fluorescence change (Fig. 8).

Structure of the L-Cu²⁺ complex (1)

In general, solid state properties may or may not be always the same with the solution phase characterisation by ESI-MS, ¹H NMR spectroscopy *etc.* Thus to isolate the host-guest complex in the solid phase, a careful attempt has been made by mixing the receptor with each analyte in pure methanolic solution in a 1 : 1 stoichiometric ratio. To our satisfaction, the single crystals of L-Cu²⁺ complex were grown by slow evaporation of the solvent at room temperature, while in a similar type of synthesis, only micro crystals of the L-Ni²⁺ complex were obtained which were not suitable for single crystal XRD studies. The L-Cu²⁺ complex (1) crystallizes in the monoclinic system with the space group *C*12/*c*1. In L-Cu²⁺, the Cu²⁺ ion assumed a square



Scheme 2 Proposed sensing mechanism of L.

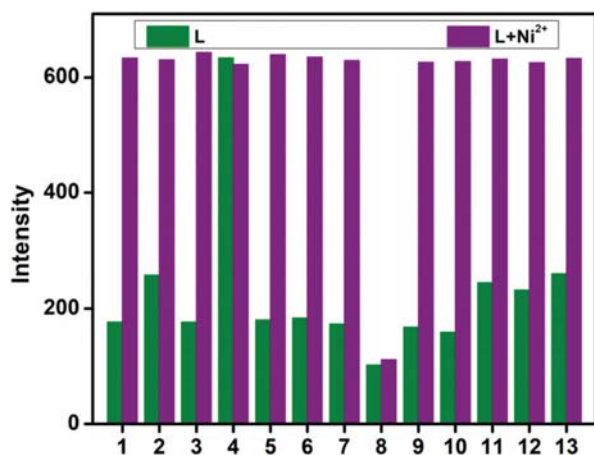


Fig. 8 Fluorescence competitive experiment in the presence of L and other metal ions (where 1 = L, 2 = Fe³⁺, 3 = Co²⁺, 4 = Ni²⁺, 5 = Cd²⁺, 6 = Hg²⁺, 7 = Pb²⁺, 8 = Cu²⁺, 9 = Ag⁺, 10 = Al³⁺, 11 = Mn²⁺, 12 = Cr³⁺ and 13 = Zn²⁺).

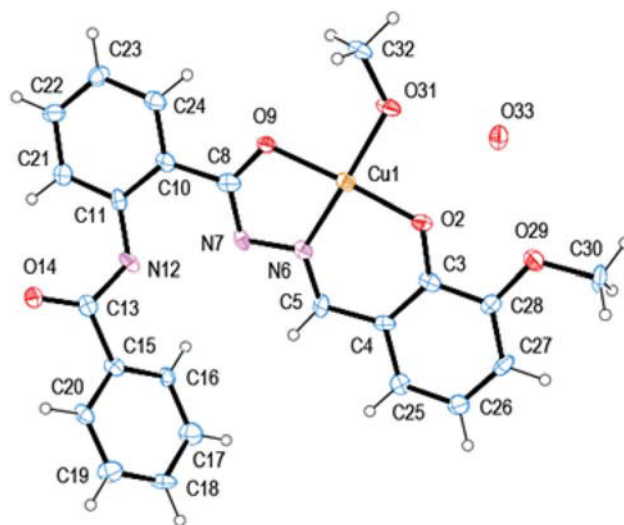


Fig. 9 Crystal structure of the L–Cu²⁺ complex (1) with 40% ellipsoid.

planar coordination geometry (Fig. 9), where the three coordination sites have been satisfied by the amide and phenoxide O atoms and the imine nitrogen atoms of the probe L and the fourth position is supplemented by the methoxide ion. The cationic charge of the Cu²⁺ ion has been internally satisfied by the –OH and –CH₃OH anionic charges. The metal centric bond angles were very close to 90° and 180° and adopted nearly a square planar geometry. The crystal structure of **1** is in agreement with the Job's plot which indicates 1 : 1 complexation (Fig. 4a) stoichiometry between L and Cu²⁺. The FTIR spectra of **1** are shown in Fig. S10.†

Stoichiometry of the L–Ni²⁺ complex (2)

In order to confirm the binding interaction between L and the Ni²⁺ ion, ¹H-NMR and FTIR spectroscopic measurements were carried out. In the NMR spectra the –OH peak at δ = 12.29 ppm completely vanished, which confirms the deprotonation in the Ni²⁺ bound state (Fig. S11†). Also the azomethine proton shifts to the down field and the amide protons become broad due to their coordination with the Ni²⁺ ion. In the IR spectra, the free receptor shows 1664 cm^{–1} (C=O) and

1612 cm^{–1} (C=N) bands along with broad bands around 3500 cm^{–1} and 3210 cm^{–1}, which were assigned to the H bonded –OH and >NH stretching vibrational modes. The vibrational bands for C=O and C=N groups shift to 1645 cm^{–1} and 1602 cm^{–1} in the L + Ni²⁺ complex due to the co-ordination of the C=O and C=N moieties with Ni²⁺ whereas a broad band around 3300 cm^{–1} appeared for the –OH group of Ni²⁺ bonded water (Fig. S12†).

DFT calculations on L, 1 and 2

We have seen that the chemosensor L crystallized in four different conformations leading to very similar structures (Fig. S13†). We have computed the energy of all crystallographically isolated conformers and listed their energy in Table S1.† The determined stability order of the conformers runs as conformer II > conformer IV > conformer I > conformer III. The optimized geometry of L is closest to the conformer II. The geometry optimized structures of L and complexes **1** and **2** are shown in Fig. 10 and the parameters of L and **1** are compared in Table S2† as a validation for the computational methodology used throughout. The calculated and

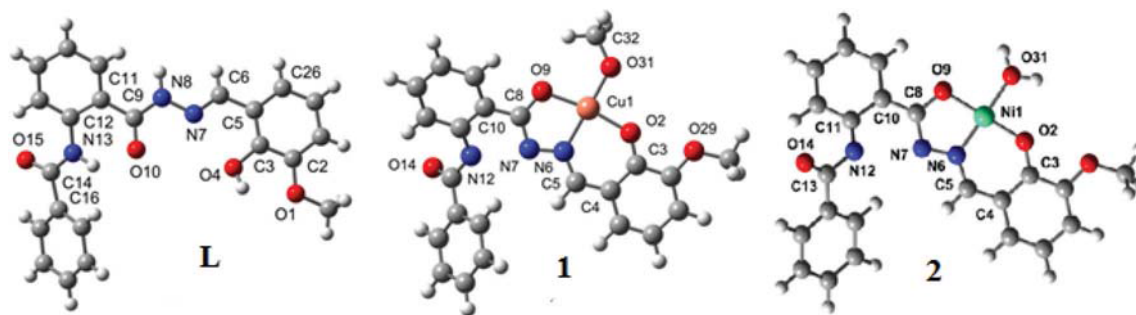


Fig. 10 DFT optimised structures of L, 1 and 2⁺.

experimental bond distances of L and 1 are in good agreement, with errors of about 0.033 Å. The errors are observed for the Cu–N6, Cu1–O2 and Cu1–O9 bond distances, for which the calculated value becomes 0.115 Å, 0.110 Å and 0.055 Å larger than the corresponding experimental values. Interestingly, the calculated Cu1–O31 bond distance is considerably shorter than the corresponding experimental value of about 0.08 Å, because of lattice effects which are not considered in the present calculations. The optimized structure of the species 2⁺ is a square planar one (Fig. 10c) and Table S3[†] represents the calculated bond distances and bond angles. The Ni–amide oxygen, Ni–phenoxo oxygen and Ni–imino nitrogen bond lengths for the optimized structure 2⁺ are found to be 1.860 Å, 1.831 Å and 1.844 Å, respectively, which are in the typical range of distances as observed in the case of some reported metal complexes with similar type ligands.⁴⁵ The Ni–O (water) bond length is observed to be 1.904 Å, similar to reported complexes elsewhere.⁴⁶ Good agreement exists between the calculated geometries of the model structures of 2⁺ and the reported square planar compounds.⁴⁷

TDDFT calculations on L, 1 and 2

The experimental and theoretical IR spectra of L and complexes 1 and 2 are presented in Fig. 11, displaying good overall agreement. Similarly, the diagnostic IR frequencies and their assignments are listed in Table S4.[†] The ligand L shows strong bands in its FTIR spectrum at 1675 and 1664 cm⁻¹, assigned

to the stretching vibration of the C=O of the amide.⁴⁸ The observed strong band at 1649 cm⁻¹ is due to the C=N vibration of the ligand. The broad band found at 3435 cm⁻¹ is assigned to the O–H stretching vibration. The amide and imine stretching frequencies decrease from 1664 and 1649 to 1590 and 1616 cm⁻¹ in 1 and 1664 and 1649 to 1642 and 1610 cm⁻¹ in 2, respectively, due to the amide and imine groups coordinated to the metal ions in 1 and 2. In complex 2, the broad band found at 3338 cm⁻¹ is assigned to the O–H and Ar–H stretching vibrations. The corresponding bending mode of water $\delta_{(H-O-H)}$ is shown at 1560 cm⁻¹. Our computed IR frequency values are found to observe within 7% of the respective experimental values. This variation is justified because the theoretical values are based on the calculations in the gas phase.⁴⁹

The absorption spectra of L, 1 and 2 are simulated in the CPCM model using the TD-DFT methods with the same hybrid basis set and functional as used in the geometry optimization calculations. The calculated spin-allowed electronic transitions with the experimental absorption spectra of L, 1 and 2 were recorded in MeOH solution. As can be seen in Fig. 12 and Table S5,[†] there is good agreement between the experimental bands and the calculated transition energies. It can be seen from the table that the experimental band observed at 294 nm is assigned to a HOMO (H) → LUMO (L) and H–1 → L transitions for L. The second experimental band, found at 220 nm, can be assigned to H–4 → L+1,

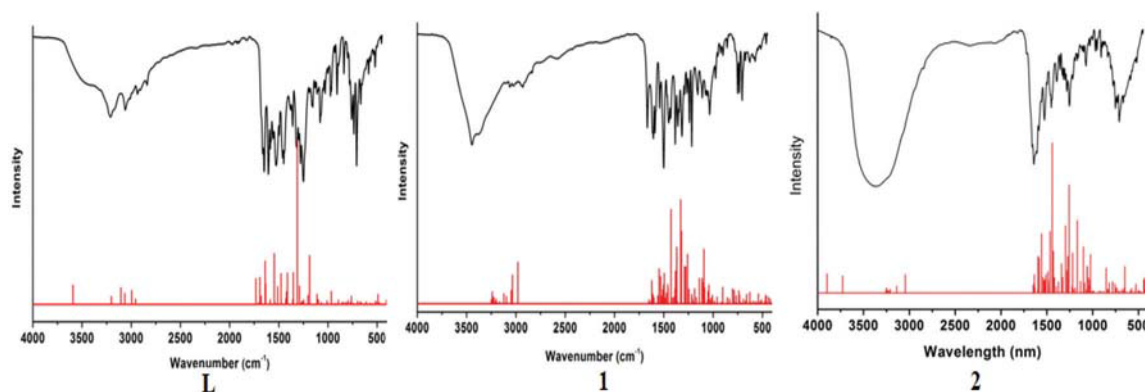


Fig. 11 The experimental (black) and calculated (red, non-scaled) vibrational spectra and the calculated vibrational transition of L, 1 and 2.

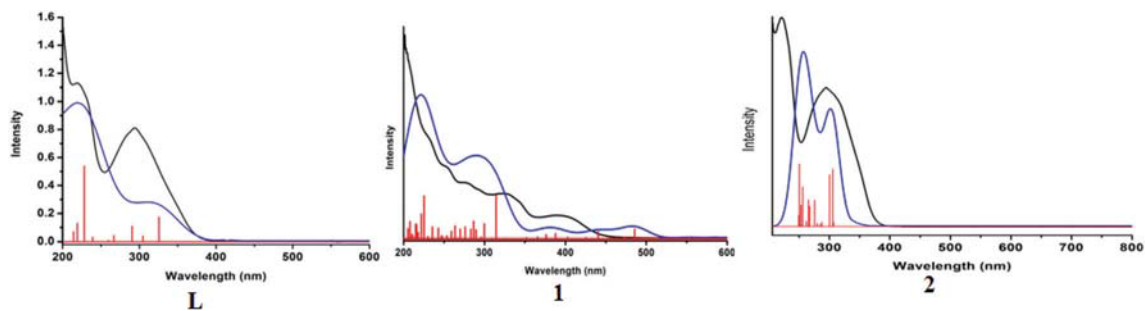


Fig. 12 The experimental (black) and calculated (red) electronic absorption spectra and the calculated electronic transition (blue) of L, 1 and 2.

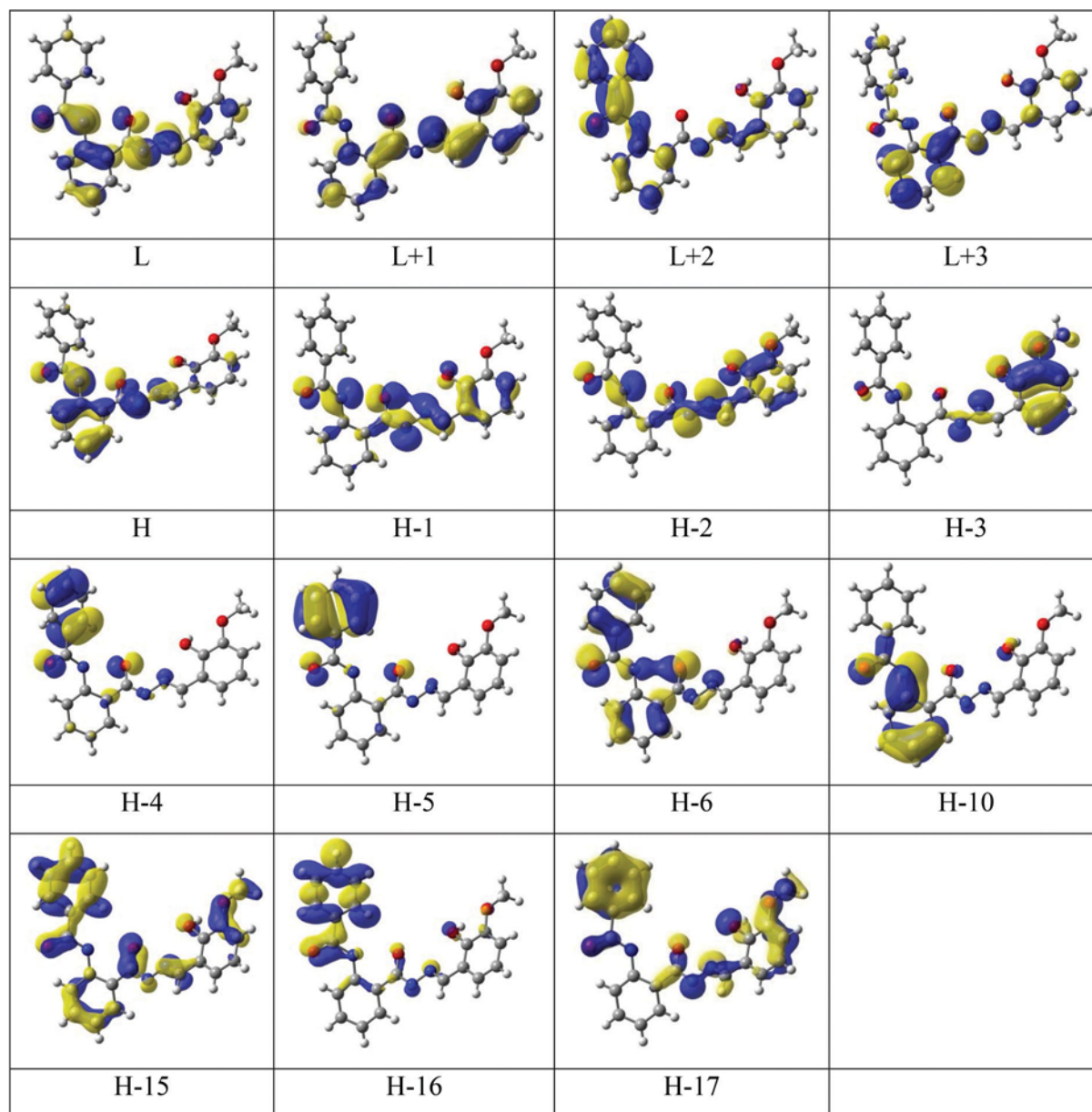


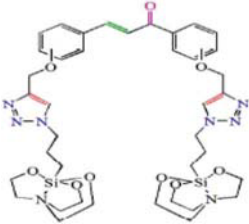
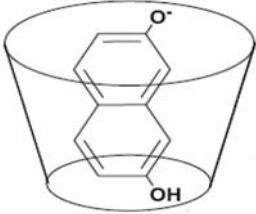
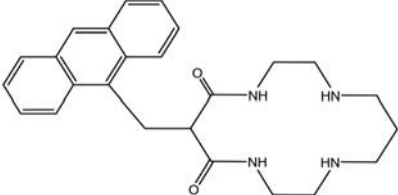
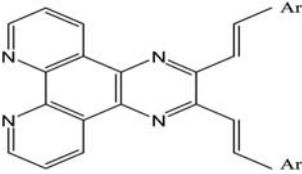
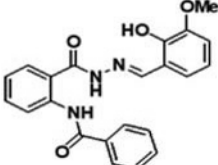
Fig. 13 Selected HOMOs and LUMOs of HL are shown. Positive values of the orbital contours are represented in yellow (0.03 au) and negative values in blue (−0.03 au).

H-16 → L, H-10 → L transitions for **L** and also the other electronic transitions as well as their frequencies. The pictorial view of the π character orbitals of HOMOs and the π^* character orbitals of LUMOs are shown in Fig. 13 for **L**. On the basis of these HOMO and LUMO molecular orbital analysis, the calculated transitions of **L** can be assigned to intra-ligand charge transfer transitions. The planarity and geometry of the ligand backbones are different in the free ligand and in the metal complexes **1** and **2**, which is reflected in the bands of absorption spectra of **L**, **1** and **2**. Table S6† shows that the experimental bands observed at 390, 325, 277, 250, 230 and 202 nm can be assigned to H → L (β) and H-3 → L+1 (β), H-1 → L (α), H → L (α), H-1 → L (β); H → L+1 (α), H-1 → L+2 (β), H → L (β), H-2 → L+1 (β), H-2 → L+1 (α); H-1 → L+1 (α), H → L+2 (β), H-10 → L+1 (β); H-3 → L+1 (α), H-2 → L+2 (β), H-4 → L+3 (β) and H-8 → L+1 (β), H-4 → L+3 (β), H-13 → L (α), H-7 → L+1 (α) transitions respectively for **1**. Thus, the

experimental bands observed at 394 and 220 nm can be assigned to H-1 → L+1, H-1 → L+2, H-7 → L+2 and H-2 → L+1, H → L+4, H-6 → L+1, H-15 → L transitions respectively for **2**.

The pictorial view of the π character orbitals of HOMOs and the π^* character orbitals of LUMOs are shown in Fig. S14 and S15;† for **1** and **2** respectively. On the basis of these HOMO and LUMO molecular orbital analysis, the calculated transitions of **1** of 390 nm and 325 nm can be assigned to the ligand to metal charge transfer (LMCT) and are correlated with the theoretically calculated electronic transitions at 485.60 nm and 387.72 nm respectively. The experimental absorption bands at 277 nm, 250 nm, 230 nm and 202 nm are in good agreement with the theoretically calculated electronic transitions at 376.04, 286.61, 235.61 and 225.27 nm respectively. Likewise, in the case of **2**, the transition at 394 nm can be assigned to the ligand to metal charge transfer (LMCT) and some contribution of d-d transitions is correlated with the

Table 2 Comparison of **L** with other previously reported dual chemosensors for Cu^{2+} and Ni^{2+} ions

Chemical structure of the probe	Binding Constant for Cu^{2+} and Ni^{2+} respectively	Sensing method	LOD for Cu^{2+} and Ni^{2+} respectively	Ref.
	4×10^4 and 1.75×10^4	Both colorimetric and fluorometric	15 μM and 20 μM	51
	1.1×10^4 and 1.75×10^4	Fluorometric		52
	1.3×10^4 and 1.1×10^4	Fluorometric	50 μM and 65 μM	53
	8.9×10^6 and 2.51×10^7	Fluorometric	3.15 μM and 6.3 μM	54
	1.3×10^4 and 1.1×10^4	Both colorimetric and fluorometric	1.8 μM and 1.7 μM	Present work

theoretically calculated electronic transition at 300.67 nm. The experimental absorption band at 220 nm is in good agreement with the theoretically calculated electronic transition at 250.60 nm. Basically, these transitions are ligand–ligand either $\pi \rightarrow \pi^*$ and/or $n \rightarrow \pi^*$ transitions. In these cases theoretical data slightly varied from the corresponding experimental data, which is reasonable, as the theoretical calculations are based on the gas phase. The theoretically calculated data are often at variance with the experimentally observed data.⁵⁰

Comparison of L with other previously reported dual chemosensors for Cu²⁺ and Ni²⁺ ions

As part of our ongoing effort on providing useful analytical techniques to monitor the increasing number of analytes of environmental relevance as quickly and as cheaply as possible and with the highest order of sensitivity, the present paper describes the synthesis of a new fluorescent-colorimetric probe L, which was validated for detection and quantification of Cu²⁺ and Ni²⁺ ions in real samples in methanol–Tris–HCl buffer solution.

To the best of our knowledge, there is no reported Schiff base which shows colorimetric and fluorometric dual selectivity for Cu²⁺ and Ni²⁺. However there are several reports where few macrocyclic and bicyclic compounds have been utilized for the selective detection of Cu²⁺ and Ni²⁺ ions. The probe, L, was compared with those reported chemosensors (Table 2). While each of the other chemosensors showed some advantages such as high sensitivity and selectivity, the important features of the fluorescent-colorimetric chemosensor, L, are easy, practical and cost effective synthesis and naked eye detection.

Table 3 Determination of Ni²⁺ and Cu²⁺ ions in water samples

Metal Ion	Spiked amount (μM)	Recovered amount (μM)	Recovery %	RSD % value
Cu ²⁺	10	9.85	98.5	1.1
	10	9.93	99.3	
	10	10.07	100.7	
Ni ²⁺	10	10.16	101.6	0.9
	10	9.98	99.8	
	10	10.11	101.1	

Application of the chemosensor L in real samples

Due to the widespread application of Cu²⁺ and Ni²⁺ ions in several laboratory and industrial purposes, it can easily enter and contaminate the aquatic ecosystem. Thus to investigate the applicability of the chemosensor L towards real water samples, artificial Ni²⁺ and Cu²⁺ contaminated samples have been prepared separately by spiking different known concentration levels, and calculated their concentrations using calibration curves (intensity ratio vs. conc.) with the help of Lambert–Beer's law (Table 3). The results obtained show good recovery measurement with RSD value less than 5% suggesting that the molecular receptor can be used to detect Cu²⁺ and Ni²⁺ ions in environmental samples.

Cell imaging study

The chemosensing ability of receptor L towards Ni²⁺ ions in the intracellular medium was also investigated by a cell imaging study using a fluorescence microscope. The selected human cervical cancer HeLa cells after incubation for 2 h at 37 °C with the receptor L and Ni²⁺ ions separately showed no fluorescence imaging when irradiated continuously at a 350 nm excitation wavelength. Under similar conditions, when the same cells were incubated with 20 μM probe L followed by 40 μM Ni²⁺ solution, a bluish green fluorescence image was observed (Fig. 14). These observations clearly indicate that the receptor L can be applicable to detect Ni²⁺ ions inside the living systems.

Molecular logic gate application

The chemosensing behaviour of the receptor L towards Cu²⁺ and Ni²⁺ ions can be applied to the formation of molecular logical devices. In the supramolecular logic gate, the analytes Cu²⁺ and Ni²⁺ ions act as dual stimulating chemical inputs whereas the output signal depended on the spectral intensity. The absorption band at around 405 nm appeared due to the action of either Cu²⁺/Ni²⁺ ion or both, mimicking the OR logical operation with a threshold value of 0.1. From the fluorescence study the emission band at around 470 nm of L–Ni²⁺, completely quenched in the presence of Cu²⁺ ions which can be utilised for the construction of INHIBIT type logic gates. The logical behaviour and the corresponding truth table are shown in Fig. 15.



Fig. 14 Fluorescence microscopy images of the HeLa cells after incubation for 2 h: (a) cells + probe L (20 μM), (b) cells + Ni²⁺ (40 μM) and (c) cells + probe L (20 μM) + Ni²⁺ (40 μM).

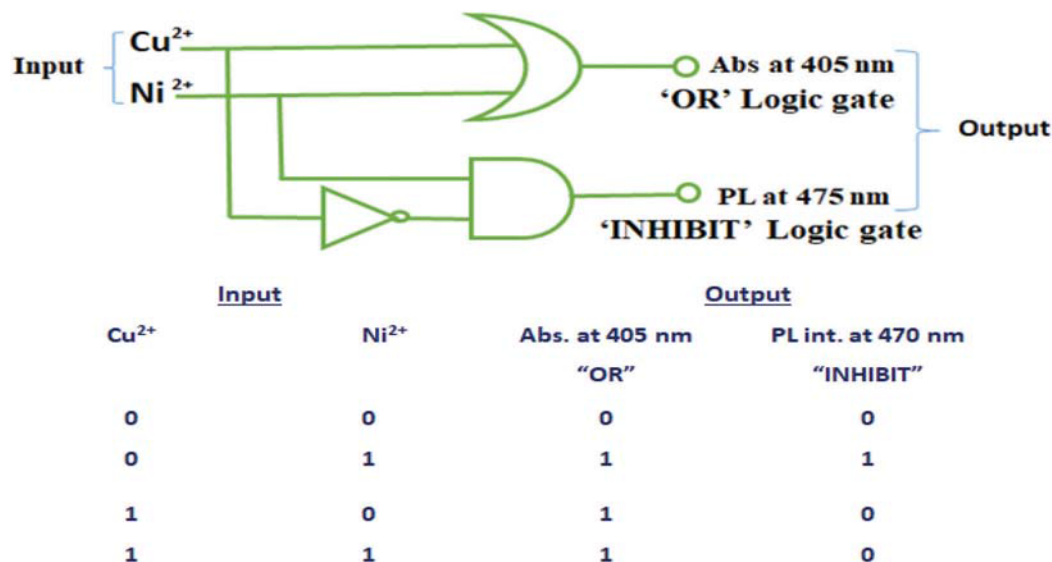


Fig. 15 Logic scheme for the proposed OR and INHIBIT type logic gates and the truth table.

Conclusion

In summary, we have successfully designed and synthesized a simple benzohydrazide based dual-mode Schiff base chemosensor **L**, for fluorescent colorimetric detection of Ni²⁺ and colorimetric detection of Cu²⁺ with high selectivity and sensitivity over other competitive ions in aqueous solution. A 1:1 stoichiometry between **L** and Ni²⁺/Cu²⁺ was supported by absorption titration, Job's plot analysis, ESI-mass spectral analysis and DFT studies. The detection limits reached up to 1.89 μM for Cu²⁺ and 1.71 μM for Ni²⁺ ions in chromogenic measurements, which were far lower than those recommended by the WHO guidelines for drinking water. The reversible responses to Ni²⁺ and Cu²⁺ ions have been established by the Na₂EDTA experiments.

Cysteine participates frequently by binding with only Cu²⁺ ions, and thus it can be used in the sensing of Ni²⁺ ions in the presence of Cu²⁺ ions. Moreover, **L** could operate in a wide range of pH values and can be successfully applied to environmental samples for detecting Ni²⁺ and Cu²⁺ ions and living cells for detecting Ni²⁺ ion. In addition, **L** can be utilized in building OR and INHIBIT types of logic gates. On the basis of these results, we believe that receptor **L** will be a remarkable supplement in the sphere of simple Schiff base sensors for multi-analytes.

Conflicts of interest

There are no conflicts to declare.

Acknowledgements

G. K. P. would like to thank the Department of Science and Technology (SR/FST/CSI-264/2014), Government of India, New

Delhi for financial support. One of the authors A. K. M. thanks the CSIR, and KR thanks DST, Government of India (No. PDF/2017/001365) for financial support in the form of research fellowships.

References

- 1 M. M. Ramon and S. Felix, *Chem. Rev.*, 2003, **103**, 4419–4476.
- 2 H. Sharma, N. Kaur, A. Singh, A. Kuwar and N. Singh, *J. Mater. Chem. C*, 2016, **4**, 5154.
- 3 D. Shan, C. Mousty and S. Cosnier, *Anal. Chem.*, 2004, **76**, 178–183.
- 4 A. Ali, H. Shen and X. Yin, *Anal. Chim. Acta*, 1998, **369**, 215–223.
- 5 M. H. Mashhadizadeh, M. Pesteh, M. Talakesh, I. Sheikhshoaie, M. M. Ardakani and M. A. Karimi, *Spectrochim. Acta, Part B*, 2008, **63**, 885–888.
- 6 S. L. C. Ferreira, A. S. Queiroz, M. S. Fernandes and H. C. dos Santos, *Spectrochim. Acta, Part B*, 2002, **57**, 1939–1950.
- 7 C. F. Harrington, S. A. Merson and T. M. D. D'Silva, *Anal. Chim. Acta*, 2004, **505**, 247–254.
- 8 S. Dadfarnia, M. A. H. Shabani, F. Tamadon and M. Rezaei, *Microchim. Acta*, 2007, **158**, 159–163.
- 9 G. K. Patra, R. Chandra, A. Ghorai and K. K. Shrivastava, *Inorg. Chim. Acta*, 2017, **462**, 315–322.
- 10 X. Zhou, S. Lee, Z. Xu and J. Yoon, *Chem. Rev.*, 2015, **115**, 7944–8000.
- 11 J. J. Lee, Y. W. Choi, G. R. You, S. Y. Lee and C. Kim, *Dalton Trans.*, 2015, **44**, 13305–13314.
- 12 A. Chowdhury, P. Howlader and P. S. Mukherjee, *Chem. – Eur. J.*, 2016, **22**, 1424–1434.

- 13 X. L. Xie, X. P. Chen, B. Li and L. M. Zhang, *Dyes Pigm.*, 2013, **98**, 422.
- 14 H. Huang, F. P. Shi, Y. Li, L. Niu, Y. Gao and S. M. Shah, *Sens. Actuators, B*, 2013, **178**, 532.
- 15 M. C. Linder and M. Hazegh-Azam, *Am. J. Clin. Nutr.*, 1996, **63**, 797–811.
- 16 R. Uauy, M. Olivares and M. Gonzalez, *Am. J. Clin. Nutr.*, 1998, **67**, 952–959.
- 17 G. Multhaup, A. Schlicksupp, L. Hess, D. Beher, T. Ruppert, C. L. Masters and K. Beyreuther, *Science*, 1996, **271**, 1406–1409.
- 18 R. A. Løvstad, *BioMetals*, 2004, **17**, 111–113.
- 19 Y. H. Hung, A. I. Bush and R. A. Cherny, *J. Biol. Inorg. Chem.*, 2010, **15**, 61–76.
- 20 J. C. Lee, H. B. Gray and J. R. Winkler, *J. Am. Chem. Soc.*, 2008, **130**, 6898–6899.
- 21 E. Madsen and J. D. Gitlin, *Annu. Rev. Neurosci.*, 2007, **30**, 317–337.
- 22 C. Vulpe, B. Levinson, S. Whitney, S. Packman and J. Gitschier, *Nat. Genet.*, 1993, **3**, 7–13.
- 23 B. Zambelli, F. Musiani, S. Benini and S. Ciurli, *Acc. Chem. Res.*, 2011, **44**, 520–530.
- 24 S. W. Ragsdale, *J. Biol. Chem.*, 2009, **284**, 18571–18575.
- 25 R. J. Maier, *Biochem. Soc. Trans.*, 2005, **33**, 83–85.
- 26 K. S. Kasprzak, F. W. Sunderman and K. Salnikowa, *Mutat. Res.*, 2003, **533**, 67–97.
- 27 P. H. Kuck, *Mineral Commodity Summaries: Nickel*, United States Geological Survey, 2006.
- 28 W. Lee, K. A. Davis, R. L. Rettmer and R. F. Labbe, *Am. J. Clin. Nutr.*, 1988, **48**, 286–290.
- 29 X. Q. Liu, X. Zhou, X. Shu and J. Zhu, *Macromolecules*, 2009, **42**, 7634–7637.
- 30 P. Ghosh, K. Pramanik, S. Paul, P. Malpaharia, S. K. Chandra, S. K. Mukhopadhyay and P. Banerjee, *ACS Appl. Bio Mater.*, 2018, **1**, 683–692.
- 31 B. Chowdhury, M. Karar, S. Paul, M. Joshi, A. Roy Choudhury and B. Biswas, *Sens. Actuators, B*, 2018, **276**, 560–566.
- 32 A. Ghorai, J. Mondal, A. K. Manna, S. Chowdhury and G. K. Patra, *Anal. Methods*, 2018, **10**, 1063–1073.
- 33 L. Wang, D. Ye and D. Cao, *Spectrochim. Acta, Part A*, 2012, **90**, 40–44.
- 34 J. R. Lakowicz, *Fluorescence Sensing, Principles of Fluorescence Spectroscopy*, Springer, Boston, MA, 2006, 623–673.
- 35 (a) A. K. Manna, J. Mondal, K. Rout and G.K. Patra, *J. Photochem. Photobiol., A*, 2018, **367**, 74–82; (b) J. Mondal, A. K. Manna and G. K. Patra, *Inorg. Chim. Acta*, 2018, **474**, 22–29.
- 36 *SMART & SAINT Software Reference manuals, version 5.0*, Bruker AXS Inc., Madison, WI, 1998.
- 37 T. Gruene, H. W. Hahn, A. V. Luebben, F. Meilleur and G. M. Sheldrick, *J. Appl. Crystallogr.*, 2014, **47**, 462–466.
- 38 L. J. Farrugia, WinGX: An Integrated System of Windows Programs for the Solution, Refinement and Analysis for Single Crystal X-ray Diffraction Data, version 1.80.01; Department of Chemistry: University of Glasgow, 2003, *J. Appl. Crystallogr.*, 1999, 32837.
- 39 M. J. Frisch, G. W. Trucks, H. B. Schlegel, G. E. Scuseria, M. A. Robb, J. R. Cheeseman, G. Scalmani, V. Barone, B. Mennucci, G. A. Petersson, H. Nakatsuji, M. Caricato, X. Li, H. P. Hratchian, A. F. Izmaylov, J. Bloino, G. Zheng, J. L. Sonnenberg, M. Hada, M. Ehara, K. Toyota, R. Fukuda, J. Hasegawa, M. Ishida, T. Nakajima, Y. Honda, O. Kitao, H. Nakai, T. Vreven, J. A. Montgomery Jr., J. E. Peralta, F. Ogliaro, M. Bearpark, J. J. Heyd, E. Brothers, K. N. Kudin, V. N. Staroverov, R. Kobayashi, J. Normand, K. Raghavachari, A. Rendell, J. C. Burant, S. S. Iyengar, J. Tomasi, M. Cossi, N. Rega, J. M. Millam, M. Klene, J. E. Knox, J. B. Cross, V. Bakken, C. Adamo, J. Jaramillo, R. Gomperts, R. E. Stratmann, O. Yazyev, A. J. Austin, R. Cammi, C. Pomelli, J. W. Ochterski, R. L. Martin, K. Morokuma, V. G. Zakrzewski, G. A. Voth, P. Salvador, J. J. Dannenberg, S. Dapprich, A. D. Daniels, Ö. Farkas, J. B. Foresman, J. V. Ortiz, J. Cioslowski and D. J. Fox, *Gaussian 09, Revision C.01*, Gaussian Inc., Wallingford, CT, 2009.
- 40 A. D. Becke, *J. Chem. Phys.*, 1993, **98**, 5648.
- 41 P. J. Hay and W. R. Wadt, *J. Chem. Phys.*, 1985, **82**, 299.
- 42 (a) W. J. Hehre, R. Ditchfield and J. A. Pople, *J. Chem. Phys.*, 1972, **56**, 2257; (b) J. D. Dill and J. A. Pople, *J. Chem. Phys.*, 1975, **62**, 2921.
- 43 V. Barone and M. Cossi, *J. Phys. Chem. A*, 1995, **102**, 2921.
- 44 J. Tomasi, B. Mennucci and R. Cammi, *Chem. Rev.*, 2005, **105**, 2999.
- 45 (a) A. Burkhardt, A. Buchholz, H. Görls and W. Plass, *Z. Anorg. Chem.*, 2003, **639**, 2516–2520; (b) K. B. Gudasi, S. A. Patil, R. P. Bakale and M. Nethaji, *J. Mol. Struct.*, 2014, **1065**, 179–185; (c) B. Tang, X. Sun, G. Liu and H. Li, *J. Mol. Struct.*, 2010, **984**, 111–116.
- 46 L.-M. Wu, H.-B. Teng, X.-C. Feng, X.-B. Ke, Q.-F. Zhu, J.-T. Su, W.-J. Xu and X.-M. Hu, *Cryst. Growth Des.*, 2007, **7**, 1337.
- 47 (a) P. Mukherjee, C. Biswas, M. G. B. Drew and A. Ghosh, *Polyhedron*, 2007, **26**, 3121–3128; (b) D. Nakane, Y. Wasada-Tsutsui, Y. Funahashi, T. Hatanaka, T. Ozawa and H. Masuda, *Inorg. Chem.*, 2014, **53**, 6512–6523.
- 48 K. Nakamoto, *Infrared Spectra of Inorganic and Coordination Compounds*, 4th edn, Wiley, New York, 1986.
- 49 P. Saha, J. P. Naskar, S. Majumder, B. Saha, R. Ganguly, A. Bhattacharya and S. Chowdhury, *J. Chin. Chem. Soc.*, 2018, **65**, 1035–1043.
- 50 P. Saha, J. P. Naskar, A. Bhattacharya, R. Ganguly, B. Saha and S. Chowdhury, *J. Coord. Chem.*, 2016, **69**, 3033–3037.
- 51 G. Singh, J. Singh, S. S. Mangat, J. Singh and S. Rani, *RSC Adv.*, 2015, **5**, 12644–12654.
- 52 R. Kavitha and T. Stalin, *J. Lumin.*, 2015, **58**, 313–321.
- 53 L. Fabbrizzi, M. Licchelli, A. Poggi, G. Rabaioli and A. Taglietti, *Springer Ser. Fluoresc.*, 2001, **1**, 209–227.
- 54 S. Sangeetha, G. Sathyaraj, D. Muthamilselvan, V. G. Vaidyanathanb and B. Unni Nair, *Dalton Trans.*, 2012, **41**, 5769–5773.